ce/papers Proceedings in civil engineering

Ernst & Sohn A Wiley Brand

ORIGINAL ARTICLE

EUROSTRUCT

Uncertainty of the crack width model based on fracture of concrete

Vladimir Cervenka[1], Arvydas Rimkus[2], Viktor Gribniak[2], Jan Cervenka[1]

Correspondence

Vladimir Cervenka
Cervenka Consulting s.r.o.
Na Hrebenkach 55
Praha 5, 15 000
Czech Repulblic
Email: vladimir.cervenlka@cervenka.cz

[1] Cervenka Consulting s.r.o., Prague, Czech Republic
[2] Vilnius Tech, Vilnius, Lithuania

Abstract

A reliable crack width assessment is a basic part of the sustainability control of the reinforced concrete structures subjected to corrosion degradation. The uncertainty of the concrete cracking model based on a finite element method and nonlinear fracture mechanics is investigated. The parameters of numerical model, such as the finite element mesh size and amount and arrangement of reinforcement are the subject of a case study. The uncertainty of the crack width model is verified on the experimental data from the tests of reinforced concrete beams. The constitutive model of crack propagation is based on the smeared cracks. The effects of numerical discretization as well as dimensional simplification are shown.

Keywords

Smeared crack model, crack width, fracture energy, model uncertainty

Nomenclature

A_s	reinforcement area	w_{exp}	experimental crack width
b	width of cross-section	w_{max}	maximum crack width
c	concrete cover depth	w_{mean}	average crack width
d	effective depth of cross-section	w_{sim}	numerical crack width
E_s	modulus of elasticity of steel	γ	orientation factor
f_{cm}	concrete strength	ε	strain
f_y	yield strength	ε_f	fracture strain
f_u	ultimate tensile strength	θ_w	model uncertainty of crack width
G_f	fracture energy	μ_θ	mean model uncertainty of crack width
h	height of cross-section	ρ	reinforcing ratio of tensile reinforcement
L_t	crack band size	σ	normal stress in crack
M_u	ultimate bending moment	σ_s	tensile stress in reinforcement
∅	bar diameter	τ_{max}	maximum bond strength
s_{max}	maximum crack spacing	DIC	digital image correlation
s_{mean}	average crack spacing	FE	finite element
V_θ	coefficient of variation of model uncertainty	IP	integration points
w	crack opening	RC	reinforced concrete
w_c	crack opening at complete release of stress		

1 Introduction

The current state of the numerical simulations of the reinforced concrete (RC) resistance reasonably describes the ULS model uncertainty [1]. Contrarily, the SLS verification of the crack width is not the case, notwithstanding the theoretical advancements [2]. The question of the crack width model quality was investigated in the concept of the digital model serving for the simulation of performance of infrastructure in environmental conditions.

The numerical analysis used in this report employs a smeared crack approach because of its simplicity, engineering efficiency, and user-friendliness. Rashid [3], Cervenka & Gerstle [4], Bazant & Oh [5], and Rots & Blaauvendraat [6] stimulated the smeared crack model development.

Gribniak et al. [7] revealed the ability of the smeared crack model with embedded reinforcement to predict the RC beams' deformations. Further, Cervenka et al. [8] observed adequate mean crack predictions for a limited experimental database. These results demonstrated the maximum crack width underestimation and the significant coefficient of variation of 35%.

Rimkus et al. [9] employed the smeared crack model to improve the numerical efficiency of the cracking analysis. The crack width parametric analysis included the effects of the bond model, fracture energy, and finite element mesh. The study proved that the perfect bond model (without a slip on the reinforcement surface) well simulates the maximum crack width prediction and that the cracks in the concrete induce the bond slip. However, the maximum and mean crack ratio of 1.18 was significantly smaller than in the test (i.e., 1.7) and provided the overestimation of the mean crack widths. Furthermore, the model uncertainty coefficient of variation was 40%, indicating a significant scatter of the results.

The simulations presented in this chapter extend the previous solutions by using an updated experimental database and employing an enhanced solution method of strain localization in the smeared crack model. A more extensive treatment by the authors can be found in [10].

2 The crack width database

The 17 beam samples had nominally identical geometry: 300 mm height, 280 mm width, and 3280 mm length. The test beams were subjected to the four-point bending scheme with a constant moment span length of 1000 mm, as shown in Figure 1.

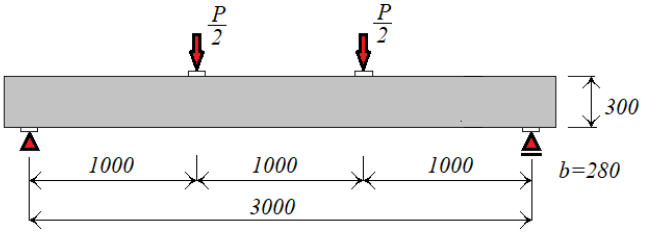

Figure 1 The loading scheme of the VILNIUS TECH tests.

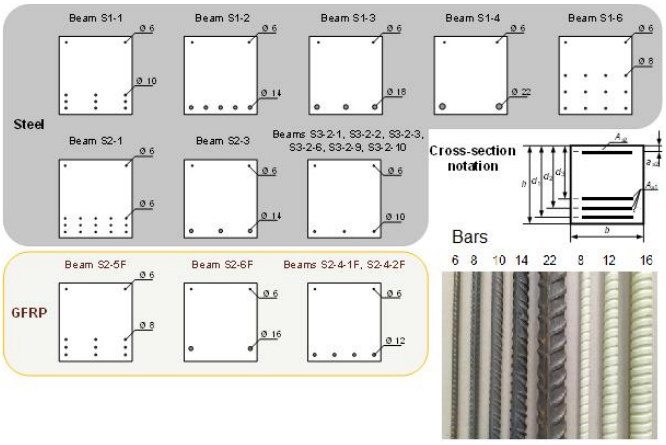

Figure 2 The loading scheme of the VILNIUS TECH tests.

The investigation object was the crack width in the constant moment zone. The investigation parameters are: reinforcement ratio, reinforcement arrangement, and material type. Two reinforcing materials are used: 13 beam specimens were provided by steel bars, and the 4 beams with the Schöck ComBAR glass fibre-reinforced polymer (GFRP) bars. Figure 2 shows the cross-sections with the reinforcement arrangement and the reinforcement surface shapes. The standard ∅150×300 mm cylinders and 280×300×350 mm unreinforced beam fragments were produced and stored together with the beam specimens to determine the concrete compressive strength and drying shrinkage deformations. All samples were made in several batches from the concrete plant with a 16 mm maximum aggregate size and a target strength 50 MPa. Table 1 and Table 2 define the cross-section geometry and mechanical parameters of reinforcement and concrete.

Table 1 VILNIUS TECH tested beams' parameters

Set	Beam	*h* mm	*b* mm	*ρ*, %	f_{cm} MPa	ε_{cs}, ‰
I		300	284	1.00	49.4	2.253
	S1-3	299	283	0.99	48.2	2.720
	S1-4	300	280	1.00	49.4	2.253
	S1-6	303	271	1.00	43.0	4.120
	S2-3	300	282	0.60	48.1	2.677
II	S3-2-1	304	278	0.30	47.7	2.230
	S3-2-2	298	283	0.30	49.5	2.851
	S3-2-3	298	284	0.30	50.9	2.109
	S3-2-6	303	279	0.30	50.9	2.240
	S3-2-9	298	285	0.30	44.2	1.970
	S3-2-10	298	284	0.30	44.6	1.970
III	S1-1	299	282	1.00	49.7	2.287
	S2-1	301	279	0.60	49.4	2.407
IV	S2-4-1F	304	273	0.60	47.2	3.177
	S2-4-2F	303	276	0.60	49.4	3.320
	S2-5F	302	276	0.67	56.0	3.787
	S2-6F	303	273	0.61	56.0	3.787

Table 2 Reinforcement characteristics

Material	∅, mm	E_r, GPa	f_y, MPa	f_u, MPa
Steel	6	223.5	585.4	642.5
	8	209.8	589.0	625.1
	10	209.9	578.1	658.5
	14	210.5	632.3	695.1
	22	199.3	551.1	553.0
GFRP	8	65.1	–	1491
	12	64.7	–	1468
	16	65.1	–	1491

In these tables, h and b are the cross-section height and width; d is the effective depth (three values correspond to the multilayer reinforcement layout; d_m is the averaged depth, corresponding to the reinforcement gravity center; a_{s2} is the compressive reinforcement depth; ρ is the reinforcement ration; f_{cm} and ε_{cs} are the compressive strength and shrinkage of concrete; ∅ is the bar diameter; E_r, f_y, and f_u are the modulus of elasticity and yielding and ultimate strengths of reinforcement. More details can be found in the references by Gribniak [11], [12]. The crack patterns of some beams after testing are shown in Figure 3. Table 3 specifies the crack values corresponding to load

P (Figure 1), representing about 50%-60% of the load-bearing capacity. This loading level is assumed as a SLS condition. The theoretical ULS load is based on the assumption of the 500 MPa for the reinforcement yielding stress (independently of the reinforcement material), Gribniak [13].

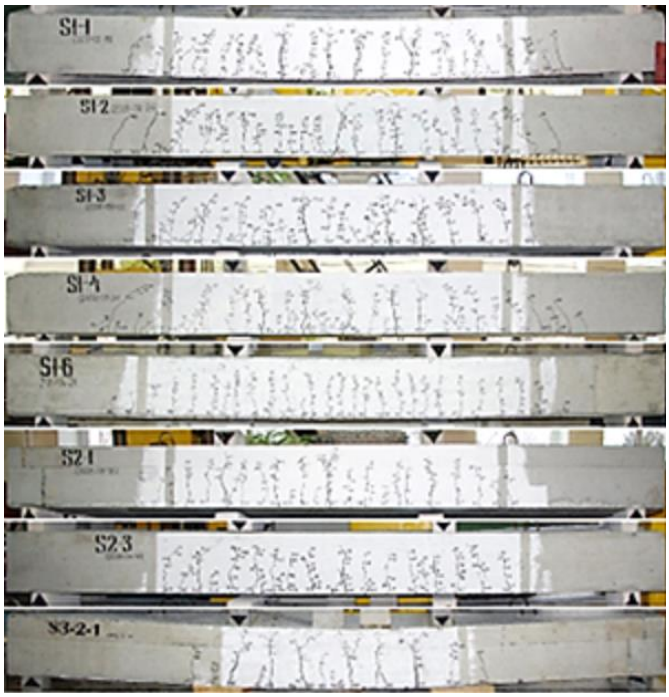

Figure 3 The crack patterns of the beams tested at the VILNIUS TECH.

Table 3 Crack width measures in the experiment.

Set	Beam	**P** kN	w_m mm×10^{-2}	w_{max} mm×10^{-2}	$\frac{w_{max}}{w_m}$
I	S1-2	124.3	7.1	10.2	1.437
	S1-3	120.2	8.5	14.0	1.647
	S1-4	100.0	6.3	12.0	1.905
	S1-6	55.9	3.8	6.0	1.579
	S2-3	76.2	5.5	12.0	2.182
II	S3-2-1	52.2	10.1	14.0	1.386
	S3-2-2	48.4	7.1	12.0	1.690
	S3-2-3	48.0	6.8	14.0	2.059
	S3-2-6	52.1	6.3	14.0	2.222
	S3-2-9	48.6	6.4	12.0	1.875
	S3-2-10	52.4	10.8	16.2	1.500
III	S1-1	96.4	9.3	12.4	1.333
	S2-1	56.2	5.9	8.2	1.390
IV	S2-4-1F	67.2	28.6	38.0	1.329
	S2-4-2F	67.3	37.6	48.0	1.277
	S2-5F	59.9	16.5	30.0	1.818
	S2-6F	49.8	15.1	48.0	3.179

2 Finite element modeling

The analysis employs the nonlinear finite element (FE) software ATENA [14]. The description of the constitutive model is limited to the tensile behavior which is relevant to the cracking problem. More details can be found in Cervenka & Papanikolau [15].

The adopted smeared crack model covers the following failure mechanisms: mode I fracture (crack opening), and mode II and III fractures (crack sliding). (For completeness, a compressive crushing of cracked concrete is also included in the model, but it does not apply to this study.) Figure 4 illustrates the mode I constitutive relation based on the crack opening law.

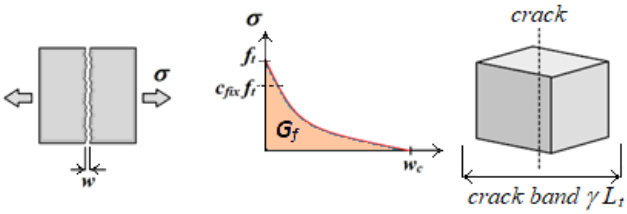

Figure 4 The crack band model.

The cohesive crack-softening model is defined according to Hordijk [16]:

$$\sigma_{ct} = f_{ctm}\left\{\left[1+\left(c_1\frac{w}{w_c}\right)^3\right]\exp\left(-c_2\frac{w}{w_c}\right)-\frac{w}{w_c}(1+c_1^3)\exp(-c_2)\right\} \quad (1)$$

where:

$$w_c = 5.14\frac{G_f}{f_{ct}};\quad c_1 = 3;\quad c_2 = 6.93. \quad (2)$$

In the above equations, σ_{ct} is the tensile stress in a crack, w is the crack width, f_{ct} is tensile strength, G_f is fracture energy.

According to the crack band model the crack width is related to fracture strain ε_f :

$$w = \varepsilon_f \gamma L_t, \quad (3)$$

where γL_t is the crack band size, L_t is a finite element size projection parallel to the crack plane, and γ is the crack orientation parameter (ranging from 1 for elements aligned with the cracks up to 1.5 for skew orientations). The fracture strain is the strain component associated with the fracture and represents damage due to cracking in terms of strains. The crack plane orientation is defined as a normal to the principal tension in concrete at the time when the principal stress in concrete reaches the tensile strength. A crack can rotate to remain coaxial with the principal tension until the threshold softening stress is reached:

$$\sigma_c = c_{fix} f_{ctm}. \quad (4)$$

where c_{fix} is a factor for the threshold limiting the rotated crack mode defining a transition from the fracture process zone to the localized crack.

The fracture modes II and III are described by the modified compression field theory, MCFT (Bentz [17]), introducing the following shear stress limit:

$$\sigma_{ij} \le \frac{0.18\sqrt{f_{cm}}(a_g+16)}{0.31a_g+4.96+24w},\quad i \ne j. \quad (5)$$

where σ_{ij} is the shear stress component on the crack surface, *i, j* are the tensor component numbers.

The softening behavior in shear is related to the mode I fracture as follows:

$$K_t^{cr} = s_F K_n^{cr},\ K_n^{cr} = \frac{\sigma_{ct}}{\varepsilon_f},\ K_t^{cr} = \frac{\tau_{ct}}{\gamma_f}\ , \quad (6)$$

where K_n^{cr}, K_t^{cr} *are* the stiffnesses of the crack opening due to the normal and shear stress, respectively, σ_{ct}, τ_{ct} are the softening stresses due to the normal and shear stress. The shear factor s_F gives a relation between the normal and shear fracture modes. In this study $s_F = 20$ *is* used. The failure modes II and III can only be activated in the fixed

crack state, since in the rotated crack mode the crack plane orientation is coaxial with the principal stress and thus without shear stress.

Cervenka et al. [18] have shown that the crack band size has limits, which are due to material heterogeneity. A very fine finite element mesh may lead to unrealistically ductile failure prediction and the minimum crack band size can overcome this problem. Bazant & Pijaudier-Cabot [19] proposed that the characteristic size can be considered for the crack band size. This study assumes the crack band limit in tension by 18 mm, which is slightly greater than the maximum size of aggregates.

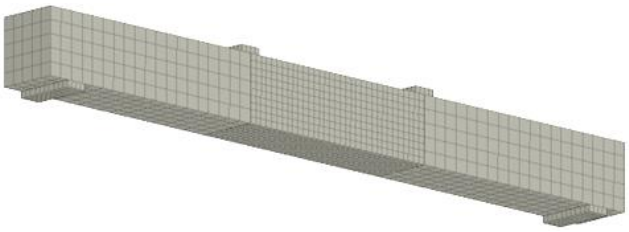

Figure 5 The 3D FE model of the beam with the mesh refinement.

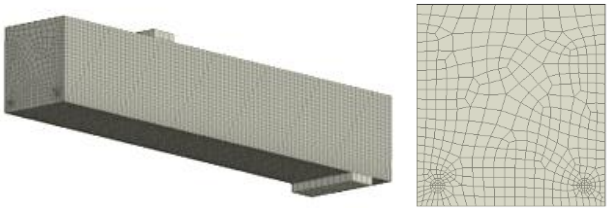

Figure 6 The 3D FE model of the beam with a 3D bar (left). Cross section (right).

Figure 5 shows the FE model employing the iso-parametric linear 3D solid brick finite elements with eight integration points. The embedded linear truss elements (1D without bending stiffness) are used for reinforcement in most cases. In addition, the parametric study includes a 2D plane stress model with iso-parametric linear quadrilateral finite elements, to investigate dimensional simplification. Furthermore, the 3D solid model for reinforcement shown in Figure 6 is investigated for S1-4 beam to demonstrate the effects of bending stiffness and of a concrete cover of the bar reinforcement.

In the central beam span, a mesh refinement was applied. This volume was connected to the end regions by a master-slave method (Jendele & Cervenka [20]). In this volume three element sizes of 60 mm, 30 mm, and 15 mm were applied. They were designated as M60, M30, and M15 in the mesh parameter study. A crack band limit of 18 mm was used in the models with mesh sizes less than 30 mm. In the above study the number of nodes ranged from 1314 (2D model with M30 mesh) to 126511 (B8 beam model with M15 mesh).

Following the findings of the previous investigation (Rimkus et al. [21]) a perfect bond model without a slip on the reinforcement surface was assumed. In this approach, the cracks in the bar vicinity simulate a bond slip.

The shrinkage for beams tested by VILNIUSTECH, Table 1, was modelled according to the laboratory data.

The tensile material parameters of concrete, tensile strength f_{ctm} and fracture energy G_f, not provided by laboratory tests, were estimated based on the *fib* Model Code MC2010 [22] formulas:

$$f_{ctm} = 0.3\sqrt[3]{f_{cm}}, \quad (7)$$

$$G_f = 73 f_{cm}^{0.18}. \quad (8)$$

An incremental solution method was based on the Newton-Raphson and line-search iteration techniques and controlled by the equilibrium criterion of 0.001 (ratio of the norm of residual forces related to the norm of external forces).

The first load increment represented the combination of the self-weight and shrinkage actions (volumetric strains uniform throughout the concrete body). The loading steps followed incrementally up to the service load level given in Table 3.

The crack width was evaluated at the integration points nearest to the monitoring line, i.e., on the surface line at the level of the tensile reinforcement gravity center. The values of mean and maximum crack widths were evaluated for each measuring line. Note that the mean crack analysis included only cracks exceeding 0.02 mm, reflecting the sensitivity of the experimental measurement.

3 Crack width uncertainty analysis

Model uncertainty of the crack width definition from the JCSS Probabilistic Model Code, [23] is adopted:

$$\theta_w = w_{exp}/w_{mod}, \quad (10)$$

where w_{exp} and w_{mod} are the measured and modeled (calculated) crack widths. The experimental crack values are listed in Table 3. The model uncertainty equal to one indicates the best modeling result. The model uncertainties in the range of $\theta_w < 1$ and $\theta_w > 1$ indicates the overestimation and underestimation of experimental results, respectively. Cervenka et al. [24] described the uncertainty of the structural resistance model applied to the ULS situation. Lindley [25] defined two uncertainty types, namely aleatory and epistemic uncertainties. The uncertainty of the theoretical model (simplifications and knowledge gaps), referred to as epistemic uncertainty is the objective of this study. The aleatory uncertainty describes the product imperfections due to geometry, treatment, material, etc. This uncertainty type is unavoidable and must be considered when estimating reliability, but it is not the objective of this study.

Table 4 The variables of parametric analysis.

Variable	Parameter
Mesh size, mm (Code)	60 (M60), 30 (M30), and 15 (M15)
The model dimensions	2D (plane stress) and 3D (volumetric)
Reinforcement ratio, %	0.3, 0.6, and 1.0
Reinforcement layout	One and three layers
Reinforcement model	1D truss, 3D solid
Reinforcement material	Steel and GFRP

The parameter study includes the beams from Table 1. The effects of the variables listed in Table 4 are investigated. The groups include samples with common characteristic parameters, which enable the identification of the uncertainty sources. The statistical parameters of the model uncertainty $\theta_{w,m}$, $\theta_{w,max}$ for the mean and maximum crack width, respectively, and for the maximum to mean crack width ratio $\theta_{x/m}$ are evaluated for each data set. Four different numerical models were applied to each set: Plane stress (2D-M30 with 30 mm mesh size) and 3D models

with three mesh sizes (3D-M60, 3D-M30, and 3D-M15).

Table 5 Crack width model uncertainty of Set I for different FE models.

Beam	2D-M30			3D-M15			3D-M30			3D-M60		
	$\theta_{w,m}$	$\theta_{w,max}$	$\Theta_{x/m}$	$\theta_{w,m}$	$\theta_{w,max}$	$\theta_{x/m}$	$\theta_{w,m}$	$\theta_{w,max}$	$\theta_{x/m}$	$\theta_{w,m}$	$\theta_{w,max}$	$\theta_{x/m}$
S1-2	1.242	2.260	1.812	0.931	0.915	0.979	1.150	0.965	0.836	0.597	0.665	1.110
S1-3	1.757	2.727	1.553	1.199	0.919	0.767	1.145	0.987	0.864	0.611	0.611	1.001
S1-4	1.351	1.626	1.205	0.795	0.804	1.012	0.862	0.970	1.126	0.580	0.626	1.079
S1-6	1.266	1.329	1.049	0.919	0.941	1.023	0.789	0.852	1.078	0.477	0.605	1.267
S2-3	1.398	2.778	1.985	1.120	1.125	1.004	0.982	1.319	1.342	0.464	0.606	1.305
Mean	1.403	2.144	1.521	**0.993**	**0.941**	**0.957**	**0.985**	**1.019**	**1.049**	0.546	0.623	1.152
CV, %	14.8	30.3	26.0	16.5	12.3	11.2	16.5	17.3	19.8	12.8	4.1	11.2

Table 6 Crack width model uncertainty of Set II for different FE models.

Beam	2D-M30			3D-M15			3D-M30			3D-M60		
	$\theta_{w,m}$	$\theta_{w,max}$	$\theta_{x/m}$	$\theta_{w,m}$	$\theta_{w,max}$	$\theta_{x/m}$	$\theta_{w,m}$	$\theta_{w,max}$	$\theta_{x/m}$	$\theta_{w,m}$	$\theta_{w,max}$	$\theta_{x/m}$
S3-2-1	3.407	3.303	0.973	1.647	0.888	0.541	2.041	1.673	0.824	0.856	0.707	0.830
S3-2-2	2.379	2.831	1.187	1.150	0.761	0.660	1.425	1.434	1.004	0.598	0.606	1.012
S3-2-3	2.295	3.303	1.446	1.110	0.888	0.804	1.375	1.673	1.223	0.577	0.707	1.233
S3-2-6	2.116	3.303	1.561	1.023	0.888	0.868	1.268	1.673	1.320	0.532	0.707	1.331
S3-2-9	2.165	2.831	1.317	1.047	0.761	0.732	1.297	1.434	1.114	0.544	0.606	1.123
S3-2-10	3.637	3.822	1.053	1.759	1.028	0.586	2.179	1.936	0.891	0.914	0.818	0.898
Mean	2.667	3.232	1.256	1.289	0.869	0.699	1.598	1.637	**1.063**	0.670	0.692	**1.071**
CV, %	25.2	11.5	18.1	25.2	11.5	18.1	25.2	11.5	18.1	25.2	11.4	18.1

Table 7 Cracking width model uncertainty of Set III for different FE models.

Beam	2D-M30			3D-M15			3D-M30			3D-M60		
	$\theta_{w,m}$	$\theta_{w,max}$	$\theta_{x/m}$	$\theta_{w,m}$	$\theta_{w,max}$	$\theta_{x/m}$	$\theta_{w,m}$	$\theta_{w,max}$	$\theta_{x/m}$	$\theta_{w,m}$	$\theta_{w,max}$	$\theta_{x/m}$
S1-1	1.730	2.260	1.211	1.444	1.345	0.933	1.862	1.277	0.687	0.884	0.867	0.982
S2-1	2.643	3.138	1.188	1.906	1.670	0.876	2.101	2.067	0.984	0.688	0.774	1.124
Mean	2.187	2.699	1.200	1.675	1.508	**0.905**	1.982	1.672	0.835	0.786	0.821	**1.053**
CV, %	29.5	23.0	1.4	19.5	15.2	4.4	8.5	33.4	25.2	17.6	8.0	9.5

Table 8 Cracking width model uncertainty of Set IV for different FE models.

Beam	3D-M15			3D-M30			3D-M60		
	$\theta_{w,m}$	$\theta_{w,max}$	$\theta_{x/m}$	$\theta_{w,m}$	$\theta_{w,max}$	$\theta_{x/m}$	$\theta_{w,m}$	$\theta_{w,max}$	$\theta_{x/m}$
S2-4-1F	2.398	1.591	0.664	1.745	1.298	0.745	0.765	0.546	0.715
S2-4-2F	3.153	2.010	0.638	2.295	1.640	0.715	1.006	0.690	0.687
S2-5F	1.345	0.883	0.658	1.032	0.978	0.950	0.382	0.438	1.147
S2-6F	1.232	2.37	1.651	0.733	0.975	1.714	0.332	0.706	2.126
Mean	2.032	1.630	0.903	1.451	1.223	1.031	0.621	0.595	1.169
CV, %	44.9	33.0	55.3	48.5	25.9	45.3	51.7	21.4	57.5

Table 9 *Prediction uncertainty summary.*

Set		2D-M30			3D-M15			3D-M30			3D-M60		
		$\theta_{w,m}$	$\theta_{w,max}$	$\theta_{x/m}$	$\theta_{w,m}$	$\theta_{w,max}$	$\theta_{x/m}$	$\theta_{w,m}$	$\theta_{w,max}$	$\theta_{x/m}$	$\theta_{w,m}$	$\theta_{w,max}$	$\theta_{x/m}$
I	Mean	1.403	2.144	1.450	**0.993**	**0.941**	**0.957**	**0.985**	**1.019**	**1.049**	0.546	0.623	1.152
	CV, %	14.8	30.3	26.0	16.5	12.3	11.2	16.5	17.3	19.8	12.8	4.1	11.2
II	Mean	2.667	3.232	1.256	1.289	0.869	0.699	1.598	1.637	**1.063**	0.670	0.692	**1.071**
	CV, %	25.2	11.5	18.1	25.2	11.5	18.1	25.2	11.5	18.1	25.2	11.4	18.1
III	Mean	2.187	2.699	1.200	1.675	1.508	**0.905**	1.982	1.672	0.835	0.786	0.821	**1.053**
	CV, %	29.5	23.0	1.4	19.5	15.2	4.4	8.5	33.4	25.2	17.6	8.0	9.5
IV	Mean				2.032	1.630	0.903	1.451	1.223	1.031	0.621	0.595	1.169
	CV, %				44.9	33.0	55.3	48.5	25.9	45.3	51.7	21.4	57.5
I-III	Mean				1.235	1.197	0.830	1.421	1.415	**1.023**	0.640	0.685	**1.100**
	CV, %				28.1	17.0	19.8	33.4	27.6	19.7	23.6	13.0	14.1

The resulting model uncertainties, indicating the predictive quality of the numerical models are summarized in Tables 5, 6, and 7, for the test Sets I, II, and III, for four models. Table 8 shows the results for Set IV for three models (3D only). The model uncertainties of the crack width simulation are summarized in Table 9.

4 Discussion of model quality

Satisfactory simulation results are manifested by a mean model uncertainty close to unity (showing a low bias), and a low coefficient of variation (consistency). These are marked in Table 5 in red color. It can be observed that the models 3D-M30 and 3D-M15, e.i. 3D models with medium and fine meshes, provide an excellent prediction for maximum and mean crack width for Set I (typical RC beams). Furthermore, the ratio w_{max}/w_m is also well reproduced.

On the other hand, the plane stress model (2D-M30) demonstrates a remarkably inferior performance, significantly underestimating the crack width and the ratio w_{max}/w_m (Table 5). A similar trend is valid for other datasets. This can be explained by the assumption of one crack throughout the beam thickness in the plane stress model. Therefore, the 2D modeling concept is not recommended for the cracking analysis, though it can represent the deformation response adequately (Gribniak et al. [7]).

Set II (Table 6) of six nominally identical beams demonstrates the evidence of aleatory uncertainty. The average parameters for the geometry and material of the beams are assumed in the simulation. Therefore, only one simulation is made for all beams of this data set. An improvement can be observed with the model refinement. The fine model 3D-M15 provides a maximum crack width overestimation of 15%, a mean crack width underestimation of 22%, and a ratio w_{max}/w_m overestimation of 44%. The poor performance of this data set can be attributed to the effect of material heterogeneity on the strain localization, which is dominant for the low reinforcing ratio. This was also observed by Gribniak [26]. Gribniak [27] presented a relevant example of the random nature of concrete's mechanical performance.
The coarse model 3D-M60 in all cases overestimated the maximum and mean crack width, which is essential for engineering applications and can be regarded as a conservative design check.

The effect of reinforcement arrangement is investigated in Set III with three layers of reinforcement. This effect can be observed from a comparison with the counterparts in Set I, with one layer reinforcement arrangement but the same reinforcing ratio. The analysis indicates that replacing the single-layer reinforcement arrangement with the multilayer arrangement with the small bar diameter and spacing increases the model uncertainty and indicates the crack width underestimation by about 50% for medium and fine meshes (3D-M30 and 3D-M15). This poor performance can be attributed to the composite nature of such material, where the bar interaction is dominant. Unfortunately, the small number of samples does not allow us to draw strong conclusions.

The results of Set IV with the GFRP reinforcement are shown in Table 8. In this case, the low stiffness of the reinforcement material becomes significant. Since the relation of the elastic moduli of GFRP and steel is about 1:3, the reinforcing ratio of the GFRP beams corresponds to ρ = 0.2% of the beams with the steel reinforcement. This is an even lower value than in group B. Thus, the conclusions from group B can be applied also here.

This study is based on a limited experimental database and does not allow a robust probabilistic analysis. Nevertheless, it offers indicative results and describes trends. It offers a general approach for quantification of the model uncertainty for the crack width prediction by nonlinear analysis, which can be quantitatively extended by adding more samples. The safety format approach proposed by Cervenka [28] can be applied with a reliability index relevant to the serviceability limit state.

4 Cracking simulation of typical beams

Beam S1-4 from Set I is chosen to illustrate the cracking simulation. It is reinforced with two 22 mm bars in a single layer with a reinforcing ratio of 1% and 20 mm cover depth. The model with a 1D bar is neglecting the bending stiffness and considers the concrete cover 31 mm. The model with a 3D bar considers the bending stiffness and the real cover size of 20 mm.

A crack formation starts at the early loading stage, where the diffused microcracks appear followed by the formation of discrete cracks, see Figure 7. (Documented also by Jakubovsis [29]). Although the simulated crack pattern agrees with the experiment there is a difference in the process of crack propagation. The crack widths at the load level P=36 kN w=0.014 mm and 0.038 mm, in the experiment and simulation, respectively, are different due to the rate of the cracking process, which is gradual in an experiment and sudden in the simulation. This is reflected in the load–displacement curves in Figure *8*. This difference was previously observed by the authors Cervenka et al. [30] and can be justified by the material heterogeneity, which is not accounted for in the simulations.

The overall load-displacement response for several models is shown in Figure 9*.* It includes three 1D bar models M60, M30, and M15, and a 3D bar model M10. The offset of the load-displacement curve without shrinkage reflects a shrinkage effect. It brings the maximum crack width increase of 25%, which confirms the previous observations of the authors that the shrinkage must be included in analysis.

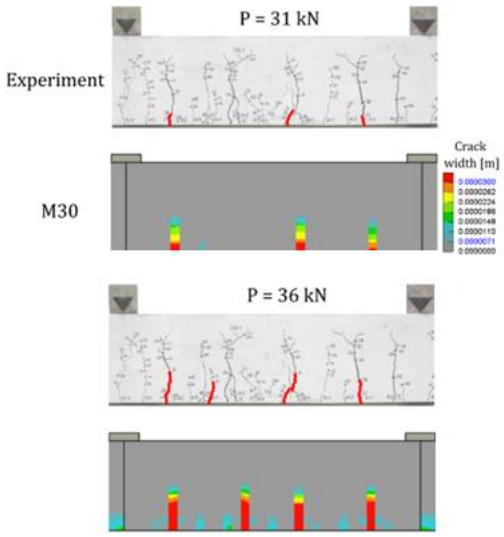

Figure 7 Crack simulation at the crack formation stage.

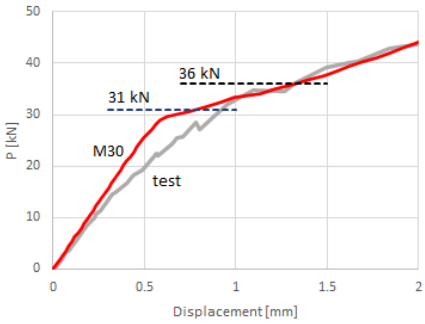

Figure 8 Load-displacement response at the crack initiation stage.

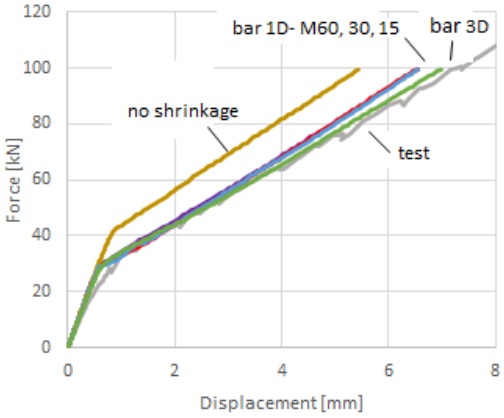

Figure 9 Overall load-displacement response of S1-4 beam from simulations and experiment.

*Fig.6.3-1*The stabilized crack pattern is analysed and compared with the experiments at the load P=100 kN in

Figure ***10***. It includes three 1D bar models M60, M30, and M15, and a 3D bar model M10. The crack patterns are shown on the concrete surface. (In the case of the model M10 with a 3D bar only a symmetrical half of the beam was modeled). The crack pattern inside of the concrete body is shown in Figure 11. for 1D M15 and 3D M10 bar models. The internal view demonstrates two types of cracks: The wide primary cracks propagate through the entire beam width, while the smaller secondary cracks, located between the primary cracks, are reflecting a concrete bond action. The secondary cracks were first described by Goto [31].

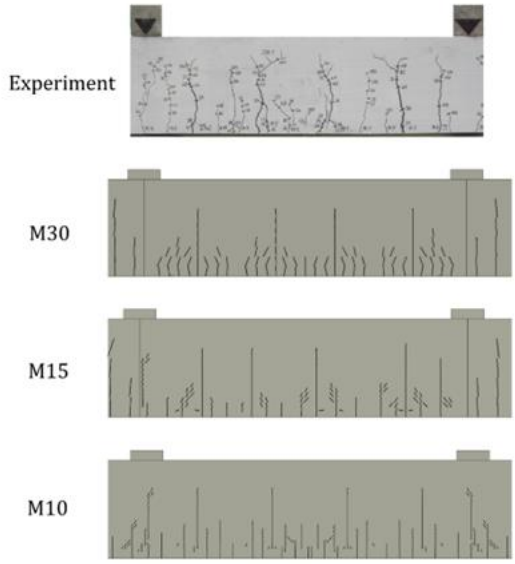

Figure 10 Experimental and simulated crack patterns, on the surface.

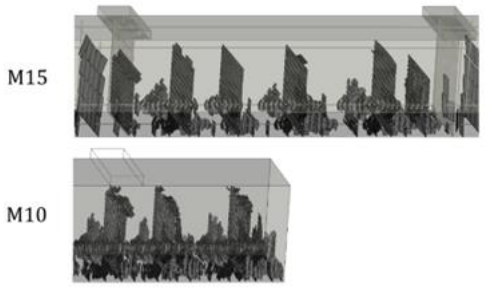

Figure 11 Inside cracks from the simulation

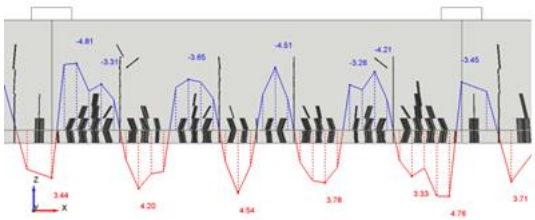

Figure 12 Bond stress distribution in 1D embedded bar of the 3D-M30 model.

The distribution of the bond stress along the 1D bar shown in Figure 12 obtained by the simulation demonstrates the stress transfer from concrete to reinforcement between the primary cracks and provides evidence for the engineering crack model, presented e.g. in the fib Model Codes. However, the presented finite element-based modeling concept overcomes the simplifying assumptions for the effective concrete area and tension-stiffening required in the engineering models.

The parameter study presented in Table 10 describes the model effects.

Table 10 Comparison of the crack width prediction for FE models of beam S1-4.

Model	R- bars	ε_{cs}, ‰	w_m	w_{max}	w_{max}/w_m
3D-M30-0		–	0.063	0.099	1.559
3D-M30	1D	2.253	0.073	0.124	1.687
3D-M15		2.253	0.080	0.149	1.877
3D-M10	3D	2.253	0.081	0.144	1.786

Table columns show subsequently: 1. Beam dimension and mesh size; 2. Bar dimension; 3. Shrinkage in ‰; 4. Mean crack width; 5. Maximum crack width; 6. Maximum to mean crack width ratio. The objective of this study is the effect of various models on the crack width. (In this case, a comparison with the experiment is not relevant since it is affected by the aleatory uncertainty.) Assuming that the model with a 3D bar 3D-M10 is the most accurate one, i.e. the target solution, the predicted mean crack width increases (prediction improves) with the model refinement. The mesh refinement from 30 mm to 15 mm brings an increase of the maximum crack width by 20% and leads to the crack width being slightly greater than the target solution. This is due to the difference in the concrete cover sizes, 31 mm in the 1D bar and 20 mm in the 3D bar, respectively. The two improvements, namely the mesh refinement within the concrete cover and the 3D bar dimension have opposite effects on the crack width. From this point of view, the 3D bar model, which represents a substantial computational demand, is not needed. However, the 3D bar model offers a better reproduction of the experimental crack pattern. It provides the best primary crack location and spacing. This is probably due to the bending stiffness, which is more realistic in the 3D bar model.

The offset of the load-displacement curve without shrinkage, shown in Figure 9, reflects a shrinkage effect. It brings the maximum crack width increase of 25%, which confirms the previous observations of Gribniak [27] that the shrinkage must be included in the analysis.

Interestingly, a low mesh effect on the beam stiffness is observed from the load-displacement curves. This is in contrast with the same effect on the crack width, where the crack width of the coarse model M60 was 40% greater than in the models M30 and M15, see Tables 5 and 6. This indicates, that the smeared crack model is more sensitive to a (local) strain localization than to an (integral) deflection.

The response of 1D bar models is slightly stiffer compared to the experiment. Almost perfect deformation fit is provided by the model M10 with the 3D bar, which can be attributed to its more realistic geometry (elimination of concrete in the volume of bars).

5 Engineering approach

The uncertainty of the engineering model is examined for the same data used in the above study to present a comparison of two modeling approaches. The two models are considered, the first one according to the fib Model Code

2010 [22], and the second one according to the fib Model Code 2020 (under preparation). These models represent the state-of-the-art level in this field. They are based on the principle of the equilibrium between the tensile stress in concrete and the bond stress and differ in the values of coefficients. The maximum crack width for the short-term loading condition and good bond performance is determined as follows:

$$w_d = \beta_w \, l_{s,max}(\varepsilon_{sm} - \varepsilon_{cm} - \varepsilon_{cs})$$

$$= \beta_w \left(kc + \frac{1}{4}\frac{f_{ctm}}{\tau_{bms}}\frac{\emptyset_s}{\rho_{s,ef}} \right) \left(\frac{\sigma_s - \beta \frac{f_{ctm}\left(1+\alpha_e \rho_{s,ef}\right)}{\rho_{s,ef}}}{E_s} - \eta_r \varepsilon_{cs} \right) \qquad (11)$$

The above expression employs the stress equilibrium condition in a cracked section when the crack spacing $s = \beta_w$ $l_{s,max}$, $l_{s,max}$ is the bond transfer length. It assumes the following empirical parameters:

$$k = 1.0; \quad \tau_{bms} = 1.8 f_{ctm}; \quad \beta = 0.6; \quad \eta_r = 0. \qquad (12)$$

In this β_w – crack spacing factor, k – concrete cover factor, τ_{bms} – bond stress, β – tension stiffening factor and η_r – concrete shrinkage factor.

The crack spacing factor is assumed as β_w=2 or 1.7 in MC 2010 and MC2020, respectively.

Balazs et al. [23] provide a more detailed explanation of this model.

The model uncertainties of maximum crack width were evaluated for beams reinforced by the steel bars using Eq. (11) and are summarized in Table 11.

Table 11 Crack width model uncertainty for MC 2010 and MC 2020

		Exper.	**MC 2010**				**MC 2020**			
Set	Beam	w_{max}	w_{max}	$\theta_{w,max}$	μ	*CV*	w_{max}	$\theta_{w,max}$	μ	*CV*
I	S1-2	0.102	0.179	0.569	0.549	0.074	0.168	0.608	0.667	0.147
	S1-3	0.140	0.238	0.589			0.209	0.670		
	S1-4	0.120	0.229	0.525			0.192	0.624		
	S1-6	0.060	0.105	0.572			0.072	0.836		
	S2-3	0.120	0.245	0.490			0.201	0.598		
II	S3-2-1	0.140	0.369	0.380	0.385	0.073	0.289	0.484	0.499	0.080
	S3-2-2	0.120	0.315	0.380			0.241	0.497		
	S3-2-3	0.140	0.332	0.421			0.252	0.556		
	S3-2-6	0.140	0.363	0.386			0.279	0.503		
	S3-2-9	0.120	0.356	0.337			0.276	0.435		
	S3-2-10	0.162	0.402	0.403			0.312	0.519		
III	S1-1	0.124	0.149	0.831	0.801	0.053	0.144	0.864	0.868	0.006
	S2-1	0.082	0.106	0.771			0.094	0.872		
All					**0.512**	**0.300**			**0.620**	**0.241**

For the recent Model Code 2020, the evaluation shows the following crack width overestimation: 50% for Set I (a typical beam with a single layer reinforcement), 100% for Set II (low reinforcing ratio in a single layer), and 15% fo Set III (multilayer reinforcement arrangement). These results indicate a trend similar to the one observed in the numerical model, although the mean uncertainty values are different.

The analysis of the data by sets reveals a systematic effect (bias) reflected in the mean uncertainty. It is highest in Set II and lowest in Set III (multilayer arrangement). This indicates a trend similar to the numerical model (Table 9) although the mean uncertainty values are different. The strong systematic effect (bias) is underlined by the low coefficients of variation of individual sets within the range of 7% and 15% for MC2010 and MC 2020, respectively.

In summary, the crack width is overestimated for the MC 2010 by 95%, and for the MC 2020 by 61%. Thus, prediction according to the recent code MC 2020 is less conservative and closer to reality for this data set. Apparently, this is due to the smaller factor β_w in the MC 2020.

6 Conclusions

The uncertainty of the crack widths model based on the numerical simulation and fracture mechanics is investigated. The numerical results based on 37 model cases are verified by the experimental data of the crack width measurements of 17 beam specimens with the following conclusions:

1. The satisfactory predictions of mean and maximum crack widths are provided for normal concrete beams with a reinforcing ratio from 0.5% to 1%, and a single-layer bar arrangement.
2. The finite element mesh size affects the crack width prediction. The acceptable prediction was found for the mesh size range from 15 mm to 30 mm, confirmed by the model uncertainties close to unity, with the coefficient of variation within 16%. The minimum crack band limit of 18 mm was used for the mesh sizes smaller than this limit.
3. For the small reinforcing ratio of 0.3%, only the fine mesh of 15 mm offered an acceptable prediction of the maximum crack width, with the overestimation by 15%, and accompanied by a low coefficient of variation of 11%.
4. The crack width in beams with GFRP bars is underestimated by 18% to 48%.
5. The simplified 2D - plane stress model underestimated the crack width predictions by 53% to 70%.
6. A reinforcement model based on the truss element without bending stiffness represents an acceptable modeling method for the cracking simulation.
7. The crack width prediction according to the Model Code 2020 is overestimated by 50%.

Acknowledgment

The research was a part of the project ID TCK03000023 "Digital twin for increased reliability and sustainability of concrete bridges", which has been co-financed with the state support of the Technology Agency of the Czech Republic and the Ministry of Transport of the Czech Republic within the TRANSPORT 2020+ Programme.

References

[1] Cervenka, V., Cervenka, J. & Kadlec, L. (2018), Model uncertainties in numerical simulations of reinforced concrete structures. *Structural Concrete*, Vol. 19, No. 6, pp. 2004-2016.

[2] Sturm, A.B., Visintin, P. & Bennett, B. (2022), A hybrid deterministic-probabilistic approach for the characteristic crack widths and crack spacings in reinforced concrete tension and flexural members. *Engineering Structures*, Vol. 256, ID: 114071, pp. 65-75.

[3] Rashid, Y.R. (1968), Ultimate strength analysis of prestressed concrete pressure vessels. *Nuclear Engineering and Design*, Vol. 7, pp. 334-344.

[4] Cervenka, V. & Gerstle, K. (1972), Inelastic Analysis of Reinforced Concrete Panels: Experimental verification and Application. *IABSE Publications*, Vol. 32, pp. 26-39.

[5] Bazant, Z.P. & Oh, B.H. (1983), Crack band theory for fracture of concrete. *Materials and Structures*, Vol. 16, No. 3, pp. 155-177.

[6] Rots, J.G. & Blauvendraat, J. (1989), Crack models for concrete: discrete or smeared? Fixed, multi-directional or rotating? *Heron*, Vol. 34, No. 1, pp. 5-56.

[7] Gribniak, V., Cervenka, V. & Kaklauskas, G. (2013), Deflection prediction of reinforced concrete beams by design codes and computer simulation. *Engineering Structures*, Vol. 56, pp. 2175-2186.

[8] Cervenka, V., Markova, J., Mlcoch, J., Perez Caldentey, A., Sajdlova, T. & Sykora, M. (2018), Uncertainties of crack width models, in Proceedings of the 15th *fib* Symposium "High Tech Concrete: Where Technology and Engineering Meet", Hordijk, D.A. and Lukovic, M. (Eds.), Springer, pp. 1653-1661.

[9] Rimkus, A., Cervenka, V., Gribniak, V., Cervenka, J. (2020), Uncertainty of the smeared crack model applied to RC beams. Engineering Fracture Mechanics, Vol. 233, ID: 107088, 15 p.

[10] Cervenka, V., Rimkus, A., Gribniak, V., Cervenka, J., 2022. Simulation of the Crack Width in Reinforced Concrete Beams Based on Concrete Fracture. Theoretical and Applied Fracture Mechanics, 121 (2022) 103428.

[11] Gribniak, V., Kaklauskas, G. & Bacinskas, D. (2009), Experimental investigation of shrinkage influence on tension stiffening of RC beams, in Proceedings of the Eighth International Conference: Creep, Shrinkage and Durability of Concrete and Concrete Structures (ConCreep 8), Ise-Shima, Japan, 2008. CRC Press/Balkema, Vol. 1, pp. 571-577.

[12] Gribniak, V., Caldentey, A.P., Kaklauskas, G., Rimkus, A. & Sokolov, A. (2016), Effect of arrangement of tensile reinforcement on flexural stiffness and cracking. *Engineering Structures*, Vol. 124, pp. 418-428.

[13] Gribniak, V., Kaklauskas, G., Torres, L., Daniunas, A., Timinskas, E. & Gudonis, E. (2013), Comparative analysis of deformations and tension-stiffening in concrete beams reinforced with GFRP or steel bars and fibers, *Composites Part B: Engineering*, Vol. 50, pp. 158-170.

[14] Cervenka Consulting (2021), ATENA program documentation, Part 1. Theory. Available at www.cervenka.cz.

[15] Cervenka, J. & Papanikolau, V.K. (2008), Three-dimensional combined fracture-plastic material model for concrete. *International Journal of Plasticity*, Vol. 24, No. 12, pp. 2192-2220.

[16] Hordijk, D.A. (1991), Local Approach to Fatigue of Concrete. PhD Thesis, Delft University of Technology, The Netherlands, 216 p.

[17] Bentz, E.C., Vecchio, F.J. & Collins, M.P. (2006), Simplified modified compression field theory for calculating shear strength of reinforced concrete elements. *ACI Structural Journal*, Vol. 103, No. 4, pp. 614-624.

[18] Cervenka, J., Cervenka, V. & Laserna, S. (2018), On crack band model in finite element analysis of concrete fracture in engineering practice. *Engineering Fracture Mechanics*, Vol. 197, pp. 27-47.

[19] Bazant, Z.P. & Pijaudier-Cabot, G. (1989), Measurement of characteristic length of non-local continuum. *ASCE Journal of Engineering Mechanics*, Vol. 115, No. 4, ID: 23365, 27-32 p.

[20] Jendele, L. & Cervenka, J. (2009), On the solution of multi-point constraints - application to FE analysis of reinforced concrete structures. *Computers and Structures*, Vol. 87, Nos. 15-16, pp. 970-980.

[21] Rimkus, A., Cervenka, V., Gribniak, V., Cervenka, J. (2020), Uncertainty of the smeared crack model applied to RC beams. Engineering Fracture Mechanics, Vol. 233, ID: 107088, 15 p.

[22] *fib* (International Federation for Structural Concrete) (2013), *Model Code for Concrete Structures 2010*, Wilhelm Ernst & Sohn, Berlin, 434 p.

[23] JCSS Probabilistic Model Code, 2001.https://www.jcss-lc.org/jcss-probabilistic-model-code/

[24] Cervenka, V., Cervenka, J. & Kadlec, L. (2018), Model uncertainties in numerical simulations of reinforced concrete structures. *Structural Concrete*, Vol. 19, No. 6, pp. 2004-2016.

[25] Lindley, D.V. (2013), Understanding Uncertainty, Revised Edition, Wiley, New Jersey, 432 p.

[26] Gribniak, V. (2009), Shrinkage Influence on Tension-Stiffening of Concrete Structures. PhD Thesis, Vilnius Gediminas Technical Univerity, Lithuania, 146 p.

[27] Gribniak, V., Jakubovskis, R., Rimkus, A., Ng, P.-L. & Hui, D. (2018), Experimental and numerical analysis of strain gradient in tensile concrete prisms reinforced with multiple bars. *Construction and Building Materials*, Vol. 187, pp. 572-583.

[28] Cervenka, V. Reliability-based non-linear analysis according to *fib* Model Code 2010. *Structural Concrete* 14(1), 2013. 19-28.

[29] Jakubovskis, R., Kupliauskas, R., Rimkus, A. & Gribniak, V. (2018), Application of FE approach to deformation analysis of RC elements under direct tension. *Structural Engineering and Mechanics*, Vol. 68, No. 3, pp. 345-358.

[30] Cervenka, V., Cervenka, J., Pukl, R., Sajdlova T. (2016). Prediction of Shear Failure of Large Beam Based on Fracture Mechanics. In: 9th International Conference on Fracture Mechanics of Concrete and Concrete Structures FraMCoS-9, V. Saouma, J. Bolander and E. Landis (Eds), Berkeley, California, USA, http://framcos.org/FraMCoS-9/Full-Papers/29.pdf, 8 pages, doi: 10.21012/FC9.029

[31] Goto, Y. (1971), Cracks formed in Concrete around Deformed Tension Bars. ACI Journal, Vol. 68, pp. 244-251.